Proceedings of the 29th IASTED International Conference
Modelling, Identification and Control (MIC 2010)
February 15 - 17, 2010 Innsbruck, Austria

MULTI-OBJECTIVE DESIGN OPTIMISATION OF A CLASS OF PKMS - THE 3-DOF GANTRY-TAU

Ilya Tyapin
School of Information Technology and Electrical Engineering
The University of Queensland
Brisbane, Queensland, Australia
email: ilya@itee.uq.edu.au

Geir Hovland
Department of Engineering
University of Agder
Grimstad, Norway
email: geir.hovland@uia.no

ABSTRACT
The main contribution of this paper is the use of the evolutionary multi-objective methodology based on the complex search algorithm and geometric approaches to optimise a parallel kinematic structure. The design optimisation scheme includes the kinematic (collisions free workspace), elastostatic (Cartesian stiffness in the Y direction) and elastodynamic (first resonance frequency) properties of the PKM as the objectives. The optimisation constraints are the support frame lengths, actuator positions, end-effector's kinematic parameters and the robot's arm lengths. The optimisation results are presented in this paper.

KEY WORDS
multi-objective design optimisation, geometric methods, PKM

1 Introduction

A generalised parallel kinematic manipulator (PKM) is a closed-loop kinematic chain mechanism where the end-effector is linked to the base by several independent kinematic chains [1]. It may consist of redundant mechanisms with more actuators than the number of controlled degrees of freedom of the end-effector. The study of PKMs has been an active research field in robotics and mechanical design for a long time. From the first ideas of [2] and [3], many mechanisms and design methods have been developed. The concept of using the parallel mechanism as a special motion mechanism with 6-DOF (degree of freedom) was first presented by [2].

The kinematic/dynamic performances of a PKM highly depend on its geometry, e.g. link lengths, positions of fixed actuators, shape and size of the manipulated platform on which the **TCP** may be defined. The optimal design problems exist because of a non-finiteness of optimisation parameters, where their upper and lower limits are not fixed and depend on other parameters, the antagonism of multiple criteria and the assignment of the initial values. To reduce the computational time effort, the optimisation parameters have to be limited and analysed before the optimisation process starts. The limits of the parameters will be found logically, analytically, specified by end-user, using the normalisation methodology [4], [5] or using other design variables to limit the optimisation parameters [13]. In [13], for example, the link upper limits are found from the unreachable space detection.

A number of different optimisation criteria for parallel manipulators have been proposed in the past. The design optimisation may have many objectives which cannot be found numerically and it is a reason why most proposed optimal design procedures are focused on the optimisation of the main characteristic of the manipulator, for example, reachable workspace, conditioning and stiffness indices, vibration analysis and manipulability criteria. In [7] it is stated that a parallel manipulator with maximum possible workspace may have undesirable characteristics such as low stiffness or resonance frequencies, which means that a multi-objective optimisation is needed. As stated in [6] the optimisation process may consist of the following stages: translate the end-user wishes into numerical indices, choose the structure and choose the dimensioning. The transformation of the user's wishes into numerical performances is given by number of DOF, workspace description, geometry and mass of load, footprint of the robot, actuators, joints, stiffness, position accuracy, internal sensors, dynamics and cost [6]. The priority levels have to be chosen for all performances.

The complex search method was used for the mechanical design optimisation in [8] and [9]. In [9] a mechanical design optimisation of a hydraulically actuated manipulator is presented. The main objective is minimising the energy consumption with side constraints on stability, response time and load dependency. The initial population has 30 designs and the optimum design is found in 250 iterations. In [8] a multi-objective design optimisation of a servo-robot for a pallets handling is presented. The objectives are the cost and speed. The accuracy of the tool point, an expected life of the planetary gears and the welded structure, vibrations and thermal conditions of the servo motors are the main side constraints. Discrete design variables originally handled by a mapping technique. The optimum design was found in 50 iterations with an initial population of 10.

Three main techniques based on the mechanism of natural selection to solve a mechanical design problem include genetic algorithms, evolution strategies and evolutionary programming. These methods are known as evolutionary algorithms. Evolutionary algorithms are suitable

for the multi-objective problem solving because they deal simultaneously with a set of possible solutions that allow to find a set of candidates for the optimal design in a single run of the algorithm instead of having to perform a series of separate runs as it deals with the traditional programming methods, for example, gradient-based search.

The multi-objective design optimisation problem is given below.

$$\begin{aligned} &\min\ [\ f_1(\mathbf{p})\ ,...,\ f_k(\mathbf{p}),\ f_{k+1}(\mathbf{p})\ ] \\ &\text{subject to} \\ &g_i(\mathbf{p}) \leq 0 \quad (1 \leq i \leq r) \\ &h_j(\mathbf{p}) = 0 \quad (1 \leq j \leq s) \\ &p_n^L \leq p_n \leq p_n^U \quad (1 \leq n \leq m) \end{aligned} \tag{1}$$

where k is the number of objective functions $f_k(\mathbf{p})$, $\mathbf{p}$ is a vector of m optimisation parameters, $g_i(\mathbf{p})$ and $h_j(\mathbf{p})$ are each of the r inequality and s equality problem constraints, p^L and p^U are lower and upper limits of the optimisation parameters. The constraints are considered as a new objective constraints handling function $f_{k+1}(\mathbf{p})$. Different constraint handling techniques are presented in [11].

The most common approach for the constrains handling is the use of penalty functions. When using a penalty function, the constraint evaluation is used to penalise an infeasible solution and feasible solutions are favored by the selection process. However, penalty functions have several drawbacks, for example, they require a careful tuning of the penalty factors that accurately estimates the level of penalisation. Also, a balance between feasible and infeasible solutions is necessary to solve a multi-objective optimisation problem and the feasible region must be wide enough to reach the global optimum.

In multi-objective optimisation, objectives are not comparable with respect to their magnitude and value and may conflict, where some objectives can not be increased without a decreasing of others. The result of a multi-objective optimisation is a set of trade-off solutions which are considered to be suitable for all objectives. In this paper the use of the evolutionary complex search algorithm for the PKM's multi-objective design optimisation is presented for the first time. The optimisation scheme includes the kinematic, elastostatic, elastodynamic properties of the machine and constraint handling based on the penalisation function.

In Section 2 the limited kinematic description of the 3-DOF Gantry-Tau parallel kinematic machine is presented. In Section 3 the basic concept of the complex search method is described. In Section 4 complex method based on geometric and functional dependency descriptions of workspace, unreachable areas, link collisions, joint angle limits, static matrix, stiffness, first resonance frequency and end-user's preferences is presented. The objective functions and constraints handling are also presented in Section 4. Section 5 contains the optimisation results and conclusions are presented in Section 6.

2 Kinematic Description

The full kinematics of the 3-DOF Gantry-Tau structure has been described earlier in [12] and [13] and limited description is presented in this paper. The manually reconfigured triangular-link version of the Gantry-Tau kinematic model is illustrated in Figs. 1 and 4. As for the basic Gantry-Tau structure, each of the 3 parallel arms (lengths L_1, L_2 and L_3) is controlled by a linear actuator with actuation variables q_1, q_2 and q_3. The actuators in Fig. 1 are aligned in the direction of the global X coordinate. The link lengths and actuator Y and Z positions are fixed.

Figs. 2 and 3 show the manipulated platform. The points A, B, C, D, E and F are the link connection points. The arm with one single link connects the actuator q_1 with platform point F. The arm with two links connects actuator q_2 with the platform points A and B. The arm with three links connects actuator q_3 with the platform points C, D and E. The triangular pair is connected to points D and E. Fig. 5 shows a projection of the link system in Fig. 1 into the XZ-plane. An angle α is a rotation about the platform Y axis which initially coincides with the global Y axis and also called the platform orientation angle.

Figs. 2 and 3 show the kinematic parameters of the moving platform. L_p is the platform length, R_p is the platform radius, β_2 is an angle between the orientation axis and positions of the points C, D, E, β_1 is an angle between the orientation axis and points A and B on the platform, β_3 is an angle between the orientation axis and the point F on the platform, d_A is the distance in the Y direction between the boundary of the platform and the point A, d_E is the distance in the Y direction between the boundary of the platform and the point E, d_{AB} is the distance in the Y direction between the points A and B on the platform, d_{ED}, is the distance in the Y direction between the points E and D on the platform, d_{EC}, is the distance in the Y direction between the points E and C on the platform. Note, that three parameters are not included into the optimisation and the end-user must specify them before the optimisation starts. These parameters are : the tool length-L_{tool}, the length from the platform circle of radius R_p to the connection point for the universal joints-L_{pin} and the length from the connection point to the centre of the joint-L_b.

Fig. 4 shows the PKM structure in both the left-hand and right-hand assembly modes. The Tau structure is characterised by a clustering of the links in groups of 1, 2 and 3, respectively, with fixed link lengths L_1, L_2 and L_3. Three linear actuators are used at the base to move the three arms independently in the global X direction. More details about the inverse and forward kinematics of the Gantry-Tau can be found in [14].

The actuator track locations are fixed in the Y and Z directions and the locations are denoted (T_{1y} T_{1z}), (T_{2y} T_{2z}) and (T_{3y} T_{3z}) respectively (see Figs. 1 and 4). The dimensioning of the PKM's support frame is given by the two variables Q_1 and Q_2 as illustrated in Fig. 4, where Q_1 is the depth and Q_2 is the height. Q_3 is the Z coordinate of the actuator T_1, Q_4 is the Y coordinate of the actuator T_2.

The width of the machine in the X direction is given by the length of the actuators. The platform points $A-F$ in the **TCP** coordinate frame are calculated as follows.

$$
\begin{aligned}
[a_x\ a_y\ a_z]^T &= R_y(\beta_1)\ [0\ (-L_{tool})\ (R_p^*)]^T \\
&\quad +[0\ (-d_A)\ 0]^T \qquad (2)\\
[b_x\ b_y\ b_z]^T &= R_y(\beta_1)\ [0\ (-L_{tool})\ (R_p^*)]^T \\
&\quad +[0\ (-L_p-d_{AB})\ 0]^T \qquad (3)\\
[c_x\ c_y\ c_z]^T &= R_y\ (180^0 \pm \beta_2)\ [0\ (-L_{tool})\ (R_p^*)]^T + ... \\
&\quad ... + [0\ (e_y+d_{EC})\ 0]^T \qquad (4)\\
[d_x\ d_y\ d_z]^T &= R_y\ (180^0 - \beta_2)\ [0\ (-L_{tool})\ (R_p^*)]^T + ... \\
&\quad ... + [0\ (e_y+d_{ED})\ 0]^T \qquad (5)\\
[e_x\ e_y\ e_z]^T &= R_y\ (180^0 \pm \beta_2)\ [0\ (-L_{tool})\ (R_p^*)]^T + ... \\
&\quad ... + [0\ (-\frac{L_p}{2}+d_E)\ 0]^T \qquad (6)\\
[f_x\ f_y\ f_z]^T &= R_y(240^0+\beta_3)\ [0\ (-L_{tool}-L_p)\ (R_p^*)]^T \qquad (7)\\
R_p^* &= R_p + L_{pin} + \frac{L_b}{2} \qquad (8)
\end{aligned}
$$

where the signs of the angle β_2 for the points E and C are the optimisation parameters, $R_p^* = R_p + L_{pin}$. The angles β_i are illustrated in Fig. 3. The matrix R_y is a standard rotational matrix.

$$
R_y(\alpha) = \begin{pmatrix} \cos\alpha & 0 & \sin\alpha \\ 0 & 1 & 0 \\ -\sin\alpha & 0 & \cos\alpha \end{pmatrix} \qquad (9)
$$

The vector pointing from the actuator position to the point A on the platform is given below.

$$
\mathbf{A} = [A_x\ A_y\ A_z]^T \qquad (10)
$$

A_x, A_y, A_z are the X-, Y- and Z- normalised components of the vector $\mathbf{A}$.

According to the kinematics, the vector from the actuator T_2 to the point A on the platform is given below. Vectors from the actuators to the points B-F are found in a similar way.

$$
\mathbf{A} = \begin{bmatrix} a_xC + a_zS + X - T_{2x} \\ a_y + Y - T_{2y} \\ a_zC - a_xS + Z - T_{2z} \end{bmatrix} \qquad (11)
$$

where $C = \cos\alpha$, $S = \sin\alpha$. The angle α is illustrated in Fig. 5. T_{2x}, T_{2y}, T_{2z} are the coordinates of actuator T_2 at the given **TCP** position, X, Y, Z are the **TCP** coordinates, $[a_x\ a_y\ a_z]$ are the coordinates of the point A in the **TCP** coordinate frame. The $\cos\alpha$ is given below.

$$
\cos\alpha = \frac{T_{3z} - Z}{\sqrt{L_{3m}^2 - (Y + M_y - T_{3y})^2} + \sqrt{M_x^2 + M_z^2}} \qquad (12)
$$

where, L_{3m} is the middle length of the triangular-mounted arm 3. M_x, M_y, M_z are coordinates of a vector from a midpoint M between the triangular link coordinates C, D and E on the platform to the actuator position $(T_{3x}T_{3y}T_{3z})$.

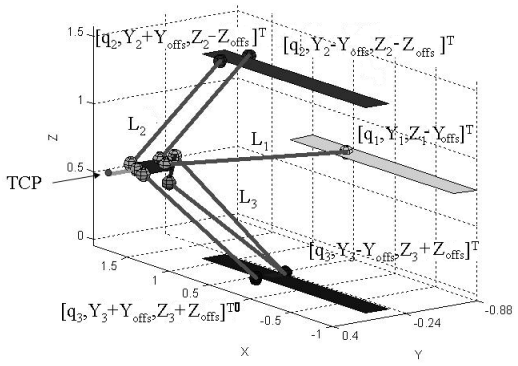

Figure 1. Triangular-link variant of the Gantry-Tau shown in the left-handed configuration for all link clusters.

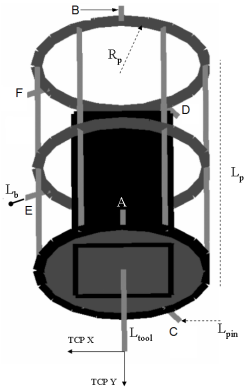

Figure 2. The manipulated platform of the Gantry-Tau.

The kinematic parameters of the prototype are presented in Section 5. X coordinates of the actuator positions q_1, q_2, q_3 are defined from general inverse kinematics and presented in [13]. A prototype of the 3-DOF Gantry-Tau with a triangular-mounted link pair built at the University of Agder, Norway is shown in Fig. 6.

3 Complex Search Method

The complex search method is based on the evolutionary multi-objective optimisation concept. In this paper the exterior penalty barrier function is used and expressed as follows.

$$
f_{k+1}(\mathbf{p}) = \sum_{i=1}^{r} G_i(\mathbf{p}) \qquad (13)
$$

where

$$
G_i(\mathbf{p}) = \left\{ \begin{array}{lll} 0 & if & g_i(\mathbf{p}) \le 0 \\ g_i^2(\mathbf{p}) & if & g_i(\mathbf{p}) > 0 \end{array} \right\} \qquad (14)
$$

Note, that $g_i(\mathbf{p})$ is normalised. A solution $g_i(\mathbf{p}) = 0$ is applied when $g_i(\mathbf{p})$ is inside of its boundaries. This barrier function eliminates any tuning parameters.

The complex search method consists of several stages:

- Generate the initial population of n designs y_n. As a rule of thumb, the size of the initial population equals

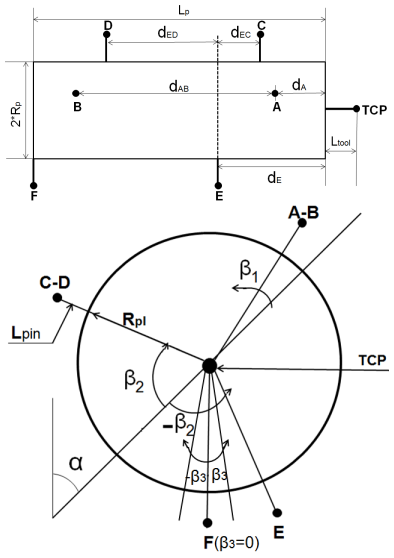

Figure 3. The sketch of the manipulated platform top view(top) and front view (bottom).

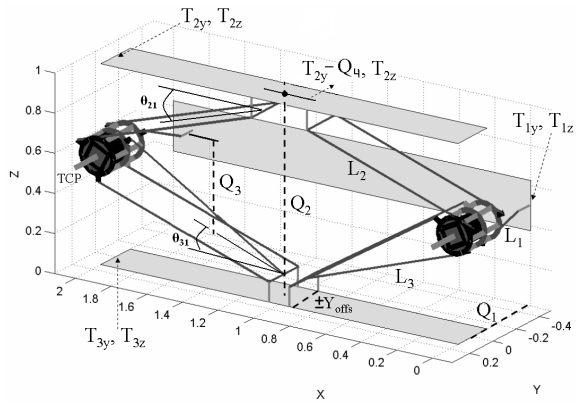

Figure 4. The 3-DOF reconfigurable Gantry-Tau robot.

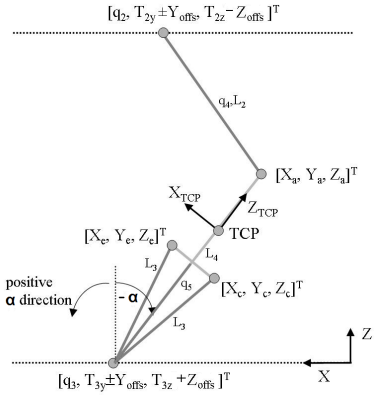

Figure 5. Kinematic parameters in XZ-plane.

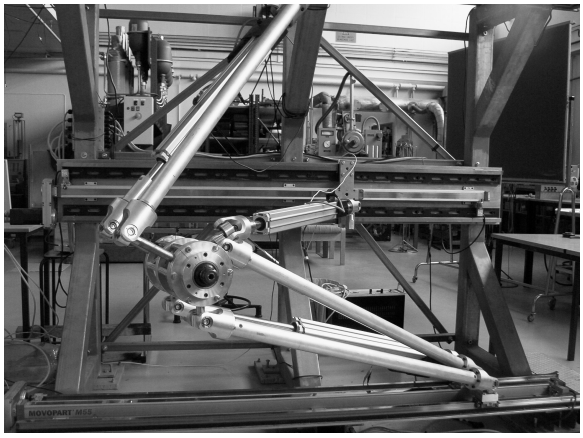

Figure 6. The Gantry-Tau prototype built at University of Agder.

m^2, where m is the number of the optimisation parameters.

- Objectives are evaluated and the worst and the best designs are identified as y_j and y_k respectively in each iteration.
- The centroid of the remaining design is found as y_c in each iteration.
- The worst design y_j is mirrored through the centroid y_c and a new design is found.
- If the new mirrored through the centroid design continues to be the worst design, it is moved towards the current best design more or less strongly depending on how often this had happened in a row.

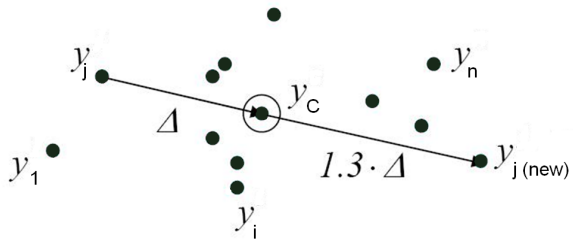

Figure 7. Complex search method. The worst design is mirrored through the centroid.

In Fig. 7 the implementation of the complex search method is shown, when a new design is found as the worst design mirrored through the centroid. The centroid y_c and a new design $y_{j\ new}$ are defined as follows.

$$y_c = \frac{\sum_{i \neq j}^{n} y_i}{n-1} \quad (15)$$

$$y_{j\ new} = 1.3(y_c - y_j) + y_c \quad (16)$$

where n is the number of the designs y and y_j is the worst design. When a new design is found through the best de-

sign, some changes are applied.

$$\varepsilon = \frac{n_0^{\frac{n_0+n_{rep}-1}{n_0}}}{n_0+n_{rep}-1} \quad (17)$$

$$y_{j\ new} = 0.5(y_j + \varepsilon y_c + (1-\varepsilon)y_k) \quad (18)$$

where y_k is the best design, n_0 is a tuning parameter, normally $4-5$, n_{rep} is the number of iterations in a row, where the design y_j has been the worst. Parameters n_0 and n_{rep} are used to switch the algorithm between the worst and the best designs to find a new one.

4 3-DOF Gantry-Tau Design Optimisation

The Gantry-Tau design optimisation problem based on the evolutionary complex search method is expressed as follows.

$$min\ \mathbf{F}(\mathbf{p}) = [\ f_{stif}(\mathbf{p})\ f_{frf}(\mathbf{p})\ f_{qual}(\mathbf{p})\ fg(\mathbf{p})\ ] \quad (19)$$

$Subject\ to$:

$Q_4^L(\mathbf{p}) \le Q_4 \le Q_4^U(\mathbf{p})$	$Q_3^L(\mathbf{p}) \le Q_3 \le Q_3^U(\mathbf{p})$
$L_3^L(\mathbf{p}) \le L_3 \le L_3^U(\mathbf{p})$	$L_2^L(\mathbf{p}) \le L_2 \le L_2^U(\mathbf{p})$
$L_1^L(\mathbf{p}) \le L_1 \le L_1^U(\mathbf{p})$	$d_E^L(\mathbf{p}) \le d_E \le d_E^U(\mathbf{p})$
$Q_1^L(\mathbf{p}) \le Q_1 \le IS_{dth}$	$Q_2^L(\mathbf{p}) \le Q_2 \le IS_{hth}$
$L_C^* \le d_{AB} \le d_{AB}^U(\mathbf{p})$	$L_C^* \le d_{ED} \le d_{ED}^U(\mathbf{p})$
$L_C^* \le d_{EC} \le d_{EC}^U(\mathbf{p})$	$0 \le d_A \le d_A^U(\mathbf{p})$
$R_{pmin} \le R_p \le R_p^U(\mathbf{p})$	$L_{pmin} \le L_p \le L_p^U(\mathbf{p})$
$0^0 \le \beta_1 \le 30^0$	$0^0 \le \beta_2 \le 90^0$
$-15^0 \le \beta_3 \le 15^0$	$tolerance = \delta^2 = 10^{-3}$

where $\mathbf{p}$ is a vector of the optimisation parameters. Each optimisation parameter has its upper and lower limits. The limits of some parameters depend on others. For example, upper $L_1^U(\mathbf{p})$ and lower $L_1^L(\mathbf{p})$ limits of the first link L_1 are the functions of the other parameters such as the angle β_3, radius of the platform R_p and user's specifications: length of the pin - L_{pin}, radius of the platform - R_p and support frame dimension in the X direction - IS_{lth}.

A vector of the 19 optimisation parameters $\mathbf{p}$ is given below and described in Section 2. Parameters β_{2E} β_{2C} are the sings and keep the direction of the angle β_2 for the points E and C on the platform.

$$\mathbf{p} = [\ R_p\ L_p\ \beta_1\ \beta_2\ \beta_3\ d_{AB}\ d_{ED}\ d_{EC}\ d_A\ d_E\ Q_1\ Q_2\ Q_3\ Q_4\ L_1\ L_2\ L_3\ \beta_{2E}\ \beta_{2C}\ ] \quad (20)$$

The user's specifications are: the minimum Cartesian stiffness k_{min} and minimum first resonance frequency γ_{min} levels specified by the user according to the robot's applications, minimum distance between two robot's links L_C^*, maximum installation space in the Y direction IS_{dth}, maximum installation space in the Z direction IS_{hth}, maximum installation space in the X direction IS_{lth}, minimum platform radius R_{pmin} , minimum platform length L_{pmin}, length from the connection point to the centre of the joint L_b, lengths of the tool L_{tool} and pins on the platform L_{pin}, Young's modulus ε_{Young}, mass of the links M_a, mass of the **TCP** M_{TCP}, mass of the joints M_j, joint stiffness k_j, individual link stiffness k_a, user's specified workspace in the Y direction UW_a and in the Z direction UW_b, workspace integration step δ. The user's specifications and requirements used in the design optimisation are given in Table 2.

The objectives vector $\mathbf{F}$ in Eq. (19) includes workspace, unreachable area, link collisions, installation space, Cartesian stiffness, dynamics performances and expressed as follows.

$$f_{stif}(\mathbf{p}) = \left\{ \begin{array}{ll} \frac{k_{min}}{k_{2,2_{min}}(\mathbf{p})}\ , & if\ Con_1 \\ 1 & ,\ if\ Con_2 \end{array} \right\} \quad (21)$$

$$f_{frf}(\mathbf{p}) = \left\{ \begin{array}{ll} \sum_{i=1}^{NUM} \frac{\delta_i^2 \gamma_{min}}{0.7\gamma_i(\mathbf{p})}\ , & if\ Con_3 \\ \sum_{i=1}^{NUM} 0 * \delta^2\ , & if\ Con_4 \end{array} \right\} \quad (22)$$

$$f_{qual}(\mathbf{p}) = \frac{IS}{A_R^*(\mathbf{p}) - \sum_{i=1}^{NUM} \frac{\delta_i^2}{0.7} A_{coll}(\mathbf{p})} \quad (23)$$

$$fg(\mathbf{p}) = \sum_{i=1}^{r} G_i(\mathbf{p}) \quad (24)$$

$$A_{coll}(\mathbf{p}) = \left\{ \begin{array}{ll} 1\ , & if\ \ link\ collisions \\ 0\ , & if\ \ no\ link\ collisions \end{array} \right\} \quad (25)$$

$$A_R^*(\mathbf{p}) = A_R(\mathbf{p}) - A_{upl}(\mathbf{p}) \quad (26)$$

$$Con_1 : K_{min} > k_{2,2_{min}}(\mathbf{p})$$

$$Con_2 : K_{min} \le k_{2,2_{min}}(\mathbf{p})$$

$$Con_3 : \gamma_{min} > \gamma_i(\mathbf{p})$$

$$Con_4 : \gamma_{min} \le \gamma_i(\mathbf{p})$$

where $k_{2,2_{min}}(\mathbf{p})$ is a minimum Cartesian stiffness in the Y direction, $\gamma_i(\mathbf{p})$ is the first resonance frequency for the current workspace cell i, $A_R(\mathbf{p})$ is the workspace, $A_{coll}(\mathbf{p})$ is the link collision parameter and equals 1 if collisions are detected or 0 if there are no collisions for the current workspace cell. All objectives subfunction's definition methods are presented in [13]. 0.7 is a parameter of the sensitivity and equals the workspace and user's specified workspace ratio, δ is the workspace integration parameter, where the minimum workspace cell equals δ^2, NUM is the number of the workspace cells, IS is the installation space and depends on the positive or negative direction of the parameter Q_4.

The weakest stiffness for the Gantry-Tau is the stiffness in the Y direction, when the single link is mounted as in Fig. 4. Increasing the stiffness in the Y direction is the main task for the stiffness optimisation. There are some solutions to increase the stiffness. The first solution is reducing the link lengths while support frame parameters Q_1, Q_2 are fixed. The second solution is increasing the parameters Q_1, Q_2 while the link lengths are fixed. The third solution to increase the stiffness is by shifting the Y position of the actuators T_2 and T_3. In this paper the Y position of actuator T_2 is variable while the actuator T_3 position is fixed. The fourth solution is a change of the distances between the points A and B or E, C and D on the platform as well as

the platform length. The last way to increase the stiffness in the Y direction is to increase Q_1 while other parameters are fixed. Note, that the support frame parameter Q_1 defines the Y coordinate of the actuator T_1. The Cartesian stiffness objective in Eq. (21) is a function of the user's requirements and optimisation parameters and equals 1 if the minimum stiffness level for the current design in the Y direction is greater than required. Apparently, the stiffness objective function is equal to the required minimum stiffness and current minimum stiffness levels ratio.

The solutions to change the first resonance frequency are the same as for the stiffness. In addition, different X and Z coordinates of the points $A-F$ on the platform will also change the first resonance frequency. However, some design modifications applied to increase the Cartesian stiffness may decrease the first resonance frequency. The balance between the optimisation parameters when both stiffness and first resonance frequency satisfy their minimum requirements on the user's specified workspace is the main task of a combined static-dynamic optimisation. The dynamics objective in Eq. (22) is a summary of the workspace cells, when the minimum required first resonance frequency is greater than a current frequency at the given cell. The dynamics objective is also extended by the ratio between the current and required frequencies, which indicates the level of the acceptance for the given cell. Apparently, the summary of the workspace cells equals zero, when the required frequency is less than the current for these cells.

Table 1. Lower and upper limits of the design parameters used in the optimisation.

$\mathbf{Par-r}$	Lower limit	Upper limit
Q_1	$\frac{UW_a}{2}+L_p+L_{tool}$	IS_{dth}
Q_2	$h_{a2}+h_{a3}+UW_b$	IS_{hth}
R_p	R_{plmin}	$\frac{IS_{hth}-UW_b}{4}$
L_p	L_{plmin}	$IS_{dth}-L_{tool}-\frac{UW_a}{2}$
d_A	0	$L_p-L_C^*$
d_E	$-\frac{L_p}{2}+L_C^*$	$\frac{L_p}{2}+L_C^*$
d_AB	L_C^*	L_p-d_A
d_ED	L_C^*	L_p+d_E
d_EC	L_p-d_E	L_C^*
β_1	0^0	30^0
β_2	0^0	90^0
β_3	-15^0	15^0

The quality objective in Eq. (23) includes the workspace, unreachable area, caused by the platform kinematic parameters, installation space and collisions detection. The installation space IS depends on the user's specifications and three support frame parameters. The workspace and unreachable area are the functions of five support frame parameters, individual link lengths and platform kinematics. In Eq. (23) the maximum reachable workspace A_R is reduced by the unreachable areas A_{upl} on its boundaries and summary of the workspace cells, where

Table 2. User's specifications and requirements used in the design optimisation.

Parameter	Volume	Parameter	Volume
k_{min}	$5\ N/\mu m$	γ_{min}	$50\ Hz$
L_C^*	$0.1\ m$	δ	$10^{-2}\ m$
IS_{lth}	$2.2\ m$	IS_{dth}	$0.65\ m$
IS_{hth}	$1.2\ m$	ε_{Young}	$70*10^9\ N/m^2$
UW_a	$0.65\ m$	UW_b	$0.65\ m$
R_{pmin}	$0.07\ m$	L_{pmin}	$0.2\ m$
k_j	$50\ N/\mu m$	k_a	$232\ N/\mu m$
M_{TCP}	$5\ kg$	M_j	$1\ kg$
M_a	$1\ kg$	L_b	$0.03\ m$
L_{tool}	$1*10^{-3}\ m$	L_{pin}	$28*10^{-3}\ m$

the collisions between the links are detected. The collisions are detected if the distance between the links is less or equal to L_C^*. If a collision between the links is detected, Eq. (25) equals 1 and workspace cell is added to the summary of the cells. The quality function is minimised while minimising the ratio between the installation space and collisions free workspace. The objective function in Eq. (24) is the constraints handling. A fully geometric method to define the optimisation parameter's upper and lower limits is given below. The limits are the functions of the user's specifications and requirements as well as the current design parameters.

The link's L_1, L_2 and L_3 lower limits are found according to Fig. 8, where $\Delta_R = R_p^* cos\beta_3$, $L_p^* = L_p + L_{tool}$ and $\Delta_{T_2} = \frac{L_p}{2} + L_{tool}$. The link's lower limits are expressed as follows.

$$L_1^L = \sqrt{(Q_1 - L_p^* + \frac{UW_a}{2})^2 + (\frac{UW_b}{2} + \Delta_R)^2} \quad (27)$$

$$L_2^L + R_p^* \sin\beta_1 = \sqrt{(\frac{UW_a}{2} + \Delta_{T_2})^2 + (\frac{Q_2 + UW_b}{2})^2} \quad (28)$$

$$\sqrt{(\frac{Q_2 + UW_b}{2})^2 + (\frac{UW_a}{2} + \Delta_{T_2})^2} = \sqrt{(L_3^L)^2 - (R_p^* \sin\beta_2)^2} - R_p^* \cos\beta_2 \quad (29)$$

where lower limits L_2^L and L_3^L are found from Eqs. (28) and (29) respectively.

The link's L_1, L_2 and L_3 upper limits are found as the maximum possible link lengths when the unreachable space in the middle of the workspace is not detected. Because of a limited space the definition method is not presented in this paper but available in [13].

In Fig. 8 the unreachable area caused by the platform kinematics is shown in dark grey colour. The light grey coloured area is the user's specified workspace. According to Fig. 8, both lower Q_3^L and upper Q_3^U limits of the Z-coordinate of the actuator T_1 are found for the given link length L_1. Both lower Q_4^L and upper Q_4^U limits of the Y-

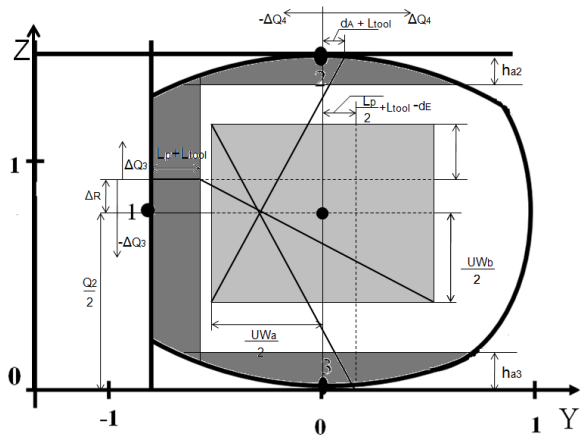

Figure 8. Definition of the link's L_1 and L_2 lower limits.

coordinate of the actuator T_2 for the given link length L_2 are found as follows.

$$L_1 = \sqrt{(Q_1 - L_p^* + \frac{UW_a}{2})^2 + (\frac{UW_b}{2} + \Delta_{Q_3})^2}$$

$$Q_3^U = \frac{Q_2}{2} - \Delta_R + \Delta_{Q_3} \quad (30)$$

$$Q_3^L = \frac{Q_2}{2} + \Delta_R - \Delta_{Q_3} \quad (31)$$

$$L_2 + R_{pl}^* \sin\beta_1 = = \sqrt{(\frac{UW_a}{2} + \Delta_{T_2} + Q_4^U)^2 + (\frac{Q_2 + UW_b}{2})^2} \quad (32)$$

$$L_2 + R_p^* \sin\beta_1 = = \sqrt{(\frac{UW_a}{2} - \Delta_{T_2} + Q_4^L)^2 + (\frac{Q_2 + UW_b}{2})^2} \quad (33)$$

The lower and upper limits of the other optimisation parameters are given in Table 1 where h_{a2} and h_{a3} are the lengths of the unreachable area shown in Fig. 8 and presented in [13].

The constraints handling method is given below.

$$g_i = 0, \quad if \ \ Par_i^L \le Par_i^{cur} \le Par_i^U \quad (34)$$

$$g_i = \left(\frac{Par_i^L - Par_i^{cur}}{Par_i^L} \right)^2, if\ Par_i^{cur} < Par_i^L \quad (35)$$

$$g_i = \left(\frac{Par_i^{cur} - Par_i^U}{Par_i^U} \right)^2, if\ Par_i^{cur} > Par_i^U \quad (36)$$

where Par_i^{cur} is a current volume of the parameter i, Par_i^U is the upper limit of the parameter i, and Par_i^L is the lower limit of the parameter i.

5 Results

The optimisation results are summarised in Table 3 and compared to original design parameters, worst and average designs. The initial population size is 300 randomised designs. The number of evaluations of the objective function was fixed to 3500. The best result was found in iteration 3169. Fig. 9 shows the convergence trend of the main objective function **F** as a summary of four sub-objectives in 3500 iterations. Fig. 10 shows the main objective function's and sub-objective's f_{qual}, f_{stif} and f_{frf} convergency trends in the last 500 iteration, where the best design was found. According to Table 3 the objective function was improved by 55 %, sub-objectives f_{qual}, f_{stif} and f_{frf} by 18.2 %, 59 % and 7.2 % respectively. The optimised design was obtained in less than 120 hours on a Pentium Centrino 2 (CPU 2.2 MHz) computer.

Table 3. Comparison of the design optimisation results.

Par − r	Original	Worst	Average	Best
Q_1 , m	0.5	0.666	0.634	0.64
Q_2 , m	1	1.221	1.022	1.126
Q_3 , m	0.42	0.474	0.481	0.452
Q_4 , m	0	−0.126	0.142	0.226
L_1 , m	1	0.954	0.996	1.092
L_2 , m	1	1.248	1.043	1.058
L_3 , m	1	0.91	0.991	1.039
R_p , m	0.08	0.146	0.093	0.091
L_p , m	0.25	0.22	0.255	0.269
β_1 , ^{0}	0	30	15.749	21.288
β_2 , ^{0}	60	80	63.156	58.039
β_{2D} , ^{0}	60	80	55.55	58.039
β_{2C} , ^{0}	60	−80	−55.55	58.039
β_{2E} , ^{0}	−60	80	55.55	−58.039
β_3 , ^{0}	0	0	−0.07	0.235
d_A , m	0	0.230	0.023	0
d_E , m	0	0.088	−0.01	−0.049
d_AB , m	0.25	−0.189	0.221	0.269
d_ED , m	0.125	0.101	0.087	0.076
d_EC , m	0.125	0.052	0.105	0.135
F	3.073	15.499	4.946	1.383
f_{stif}	2.441	1.007	1.158	1
f_{frf}	0.072	0.431	0.574	0
f_{qual}	0.468	0.56	0.883	0.383

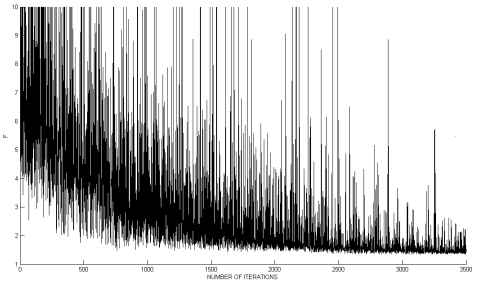

Figure 9. The main objective function as a sum of 4 sub-objectives.

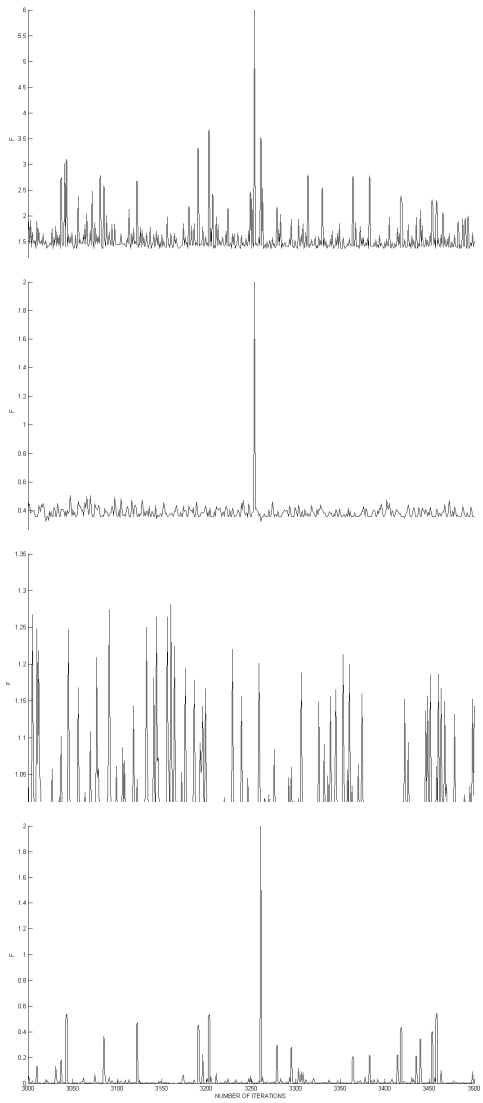

Figure 10. Last 500 iterations: main objective function (1st), the subøbjective f_{qual} (2nd), the sub-objective f_{stif} (3rd), the sub-objective f_{frf} (4th).

6 Conclusion

In order to solve multi-objective and multi-constraint problem for the PKM optimisation, the complex search method was successfully implemented with a total of 19 design parameters for the Gantry-Tau design. The constraint handling function was considered as a new objective. The user's preferences were also added into account. Furthermore, the proposed approach would be relatively simple to implement for other PKMs. Our future path of research is the use of the complex search method with a local search engine to improve its search power in order to obtain results of even higher quality at a lower computational cost.

References

[1] J.-P. Merlet, *Parallel Robots*, Kluwer Academic Publ., Solid Mech. and its Appl., Vol. 74, 2000.

[2] V. Gough, Contribution to Discussion to Papers on Research in Automobile Stability and Control and in Tire Perfomance, *Proc. Auto. Div. Inst. of Mech. Engrs*, (1956-1957), 392–394.

[3] D. Stewart, A platform With Six Degrees of Freedom, *UK Inst. of Mech. Engrs Proc.*, 180(15), 1965, 30–35.

[4] J. Cervantes-Sánchez, J. Hernández-Rodríguez, and J. Angeles, On the Kinematic Design of the 5R Planar, Symmetric Manipulator, *J. of Mech. and Mach. Theory*, 36, 2001, 1301.

[5] V. Mermertaş, Optimal Design of Manipulator With Four-Bar Mechanism, *J. of Mech. and Mach. Theory*, 39, 2004, 545.

[6] J.-P. Merlet and D. Daney, *Smart Devices and Machines for Advanced Manufacturing*, (Springer, London, 2008).

[7] R. Stamper, L. Tsai, and G. Walsh, Optimisation of a 3 DoF Translational Platform for Well-Conditioned Workspace, *Proc. IEEE Intl. Conf. on Rob. and Autmt.*, 1997, 3250–3255.

[8] M. Hansen, T. Andersen and O. Mouritsen, A Scheme for Handling Discrete and Continuous Design Variables in Multi Criteria Design Optimization of Servo Mechanisms, *Mechatronics and Robotics*, 2004, 234–245.

[9] M. Hansen and T. Andersen, A Design Procedure for Actuator Control Systems Using Optimization Methods, *Proc. of IEEE The 7th Scandinavian International Conference on Fluid Power*, 2001, 213–221.

[10] Y.-K. Hwang, J.-W. Yoon, and C. Ryu, The Optimum Design of a 6-DOF Parallel Manipulator with Large Orientation Workspace, *Proc. of IEEE Intl Conf. on Rob. and Autmt*, 2007, 163–168.

[11] C. Coello Coello, Theoretical and Numerical Constraint-Handling Techniques Used with Evolutionary Algorithms: A Survey of the State of the Art, *Comp. Meth. in Appl. Mech. and Engnrg*, 191(11-12), 2002, 1245–1287.

[12] S. Johannesson, V. Berbyuk and T. Brogårdh, A New Three Degrees of Freedom Parallel Manipulator, *In Proc. of the 4th Chemnitz Parallel Kinematics Seminar*, 2004, 731-734.

[13] I. Tyapin, *Evolutionary Multi-Objective Design Optimisation of a Class of Parallel Kinematic Machines*, Ph.D Thesis, The University of Queensland, 2009.

[14] T. Brogårdh, S. Hanssen and G. Hovland, Application-Oriented Development of Parallel Kinematic Manipulators with Large Workspace, *Proc. of the 2nd Intl. Coll. of the Coll. Res. Cen. 562: Robotic Systems for Handling and Assembly*, 2005, 153-170.